JOURNAL OF SOLID STATE CHEMISTRY **129,** 189–195 (1997)
ARTICLE NO. SC967208

Spectroscopic Studies and Crystal-Field Analyses of Am^{3+}: $LiYF_4$

R. Cavellec, S. Hubert, and E. Simoni

Institut de Physique Nucléaire (IN2P3-CNRS), 91406 Orsay, France

Received June 21, 1996; in revised form October 21, 1996; accepted October 24, 1996

Fluorescence and laser selective excitation spectroscopy have been used to investigate the electronic energy level structure of the actinide Am^{3+} ($5f^6$) in $LiYF_4$. From the analysis of the fluorescence in the visible and infrared spectra obtained at 10 K, 29 crystal-field levels have been assigned in the D_{2d} approximation. Zeeman splitting observation permits one to index some doubly degenerated Γ_5 levels. The phenomenological crystal-field parameters have been calculated in the D_{2d} approximation. A least-square adjustment yields a mean error of 38 cm^{-1} with the following values (in cm^{-1}) of the B_q^k parameters: $B_0^2 = 473$, $B_0^4 = -1776$, $B_4^4 = -2253$, $B_0^6 = 80$, and $B_4^6 = -2222$. © 1997 Academic Press

INTRODUCTION

Lithium yttrium fluoride is an interesting host material for spectroscopic studies of trivalent rare earth since it has the well known scheelite structure (1–5). In the past 15 years, it has attracted a great deal of interest as a laser host material for some lanthanide ions (Nd^{3+}, Er^{3+}, Ho^{3+}, Pr^{3+}) (6–8). Among these ions, one of the most studied has been trivalent Er^{3+} for its potential use as an infrared laser (8–10). Recently, optical spectroscopy has been investigated on single crystals of $LiYF_4$, doped with a trivalent actinide U^{3+} (11–13). Crystal-field effects on the $5f$–$5f$ transitions and intensity parametrization calculated for this system $U^{3+}/LiYF_4$ have shown that compared to the isoelectronic lanthanide ions Nd^{3+}, the ligand field induces a crystal-field about twice larger, and that the intensities of the $5f$–$5f$ transitions are ten to one hundred times stronger than the $4f$–$4f$ transitions. Moreover a continuous laser emission has been observed in the infrared region at 2.83 μm for the first time at room temperature in this system (14). Analysis of polarized absorption and fluorescence spectra at low temperature showed that the trivalent actinide U^{3+} occupies the yttrium site (S_4 symmetry) (15). Then it is interesting to study the optical properties of other trivalent actinides in this matrix. The Am^{3+} ion has the $5f^6$ configuration which is isoelectronic with Eu^{3+}. The main difference in their optical properties arises from smaller values of the Slater F^k parameters for the Am^{3+} ion and from the spin–orbit coupling ζ and crystal-field strength which are both about twice as large as for Eu^{3+} (16). Recently, fluorescence properties of Am^{3+} in fluoride glasses (17, 18) and detailed crystal-field analyses of Am^{3+} and Cm^{3+} ions in the cubic symmetry site O_h of ThO_2 (19, 20) have been reported. Other analyses of optical spectra of Am^{3+} were investigated as well in halide compounds such as $LaCl_3$ (21) and Cs_2NaYCl_6 (22, 23) where the actinide ion occupies respectively the D_{3h} symmetry and the O_h symmetry site. Therefore, it is interesting to carry out a spectroscopic study of the Am^{3+} ion in another symmetry site such as S_4 (D_{2d}) in the $LiYF_4$ host lattice. Am^{3+} (0.98 Å) has a smaller ionic radius than U^{3+} (1.028 Å), and then this actinide should replace Y^{3+} ion at the S_4 site without any distortion.

Lithium yttrium fluoride must be prepared under controlled atmosphere to avoid the presence of oxyfluorides. Because of handling radioactive elements such as ^{241}Am in a glove box, samples of $LiYF_4$ doped with Am^{3+} were synthesized as crystalline powder.

In this paper, we report the emission and excitation spectra of Am^{3+} in $LiYF_4$. Probably due to the smaller photon cutoff in fluoride matrices, numerous fluorescences were observed for the first time in the infrared from 0.9 to 1.5 μm. The large number of the lines in the fluorescence spectra in the visible and in the infrared, mainly due to transitions originating from the $^5D_1$ multiplet to the ^7F_n multiplets ($n = 0, 1, 2, 3, 4, 5$), allow us to assign 19 levels from the ^7F ground term. Unlike the isoelectronic lanthanide Eu^{3+}, for which most of the transitions involved in the fluorescence spectra are coming from the lowest excited state $^5D_0$, in the case of Am^{3+} most of the transitions originate from the $^5D_1$ state which is about 5000 cm^{-1} above the highest energy $^7F_6$ multiplet (19, 20). As a matter of fact, the spin–orbit coupling interaction is about twice as large in the actinides as in the lanthanides. Then, some levels are shifted toward the lower energies and particularly the $^5D_0$ level which is located in the same region as the $^7F_6$ multiplet.

The radiative decay constant of the emitting levels $^5D_1$ and $^5L_6$ has been measured, and the fluorescence properties of Am^{3+} in $LiYF_4$ are compared to other compounds such

0022-4596/97 $25.00

as $LaCl_3$, ThO_2, and Cs_2NaYCl_6. Zeeman experiments have been performed to assign the doubly degenerated levels Γ_5. Most of the crystal-field levels could be assigned from the selection rules in the D_{2d} symmetry. The parameters describing the spin–orbit coupling and the crystal-field interactions were adjusted using a least square minimization procedure in the D_{2d} point group approximation.

EXPERIMENTAL PROCEDURE

A sample of $LiYF_4$ doped with Am^{3+} was synthesized as powder. Pure single crystals of $LiYF_4$ were ground and melted at 850°C in a muffle furnace under circulation of argon gas. After 10 min, 200 µl of fluorhydric acid 6 *M*, in which americium oxide had been dissolved, was added to the melt. After 10 min, the temperature of the furnace was decreased slowly for 2 h from 820°C down to 750°C to ensure a good recrystallization of the sample. The isotope ^{241}Am, which has a half-life of 433 years, was used as a dopant. Because of the high specific activity of the isotope, the sample was prepared in a glove box. The Am^{3+} concentration was estimated to be roughly 10^{-2} mol%. The radioactive Am^{3+} sample was then ground and sealed in a quartz tube with parallel walls under a partial pressure of helium. Beforehand, the same procedure was tested in the well known system $LiYF_4$–Eu^{3+}. X-ray diffraction was used before and after doping, to check the structure of the matrix. No change was observed in the X-ray diffraction pattern. The luminescence spectra of the Eu^{3+} doped sample was obtained, showing the presence of only one site, from the $^5D_0 \rightarrow {}^7F_0$ transition corresponding to the Y site.

Fluorescence spectra were recorded between room and liquid temperature and analyzed with a 1-m JOBIN-YVON HR 1000 monochromator with a dispersion of 8 Å/mm. Fluorescence between 400 and 930 nm was detected using an Hamamatsu R 636 photomultiplier, while fluorescence from 800 to 2000 nm was detected either by a PbS photoresistor or by an InGaAs detector. In the infrared, the signal was measured after a Model SR510 STANFORD lock in amplifier. Quantel Nd-YAG laser pumped dye laser (pulse length 7 ns and linewidth 0.1 cm^{-1}) was used as excitation source. All of this experimental setup was controlled by a PC. The sample was placed in a liquid-helium optical cryostat (OXFORD Instruments) with a regulated, heated-gas system allowing the temperature to be varied between 10 and 300 K. The monochromator was calibrated throughout the region investigated by employing a mercury lamp. Wavelength calibration of the dye laser was verified using the calibrated monochromator. Decay times of the emitting levels were measured using a Lecroy 9350M multichannel analyzer.

The Zeeman splitting was recorded using a crysogenic superconducting magnet delivering a magnetic field up to 6 T.

THEORY AND SYMMETRY CONSIDERATIONS

The crystal structure of $LiYF_4$ is the well-known scheelite structure, where the Am^{3+} ions are substituted into the S_4 symmetry site of the Y^{3+} ions. Nevertheless, several analyses of the crystal-field parameters of rare earth ions in the scheelite structure, calculated in D_{2d} and S_4 symmetry (1, 2, 15), have clearly shown that taking D_{2d} symmetry as S_4 symmetry is a good approximation. More recently we have analyzed as well as the crystal-field of $U^{3+}/LiYF_4$ in the D_{2d} approximation (15) with a rather good agreement between the experimental and calculated levels. Thus, it is possible to neglect the imaginary part of the crystal-field parameters (B_6^4 and B_4^6). Then, the crystal-field Hamiltonian in a D_{2d} site can be written as

$$H_{CF} = \sum_{k=2,4,6} B_0^k C_0^k + \sum_{k=4,6} B_4^k (C_4^k + C_{-4}^k).$$

Using the $|5f^6, LSJM_J\rangle$ waves functions, as basis set, the electronic energy levels were fitted by simultaneous diagonalization of the free ion and crystal-field Hamiltonians H_{FI} and H_{CF} where

$$H_{FI} = \sum_{k=2,4,6} f_k F^k + \zeta_{5f} \sum_i s_i l_i + \alpha L(L+1) + \beta G(G_2 + \gamma G(R_7) + \sum_{k=2,4,6} p_k p^k + \sum_{k=0,2,4} m_k M^k + \sum_{k=2,8,k\neq 5} t_k T^k.$$

The F^k and ζ represent respectively the radial part of the electrostatic and spin–orbit interaction between 5*f* electrons; α, β, and γ are associated with the two-body effective operators of the configuration interaction and the T^k's are the corresponding parameters for the three body configuration interactions. The M^k parameters arise from the spin–spin and spin–orbit interactions, while the P^k parameters represent electrostatic spin–orbit interaction with higher configurations. The T^k, M^k, and P^k are the radial parts of the interactions, whereas the t_k, m_k, and p_k are the corresponding angular parts. For the different interaction, mechanisms present in the angular parts can be evaluated exactly, while the radial portions are treated as parameters.

The transitions or states will be described by refering to either the free-ion *J* states and/or the D_{2d} symmetry irreducible representations. In D_{2d} symmetry, the crystal-field levels are either singlet (Γ_1, Γ_2, Γ_3, Γ_4) or doublets (Γ_5). All crystal-field states from the various *J* multiplets may be classified by these symmetry labels. The lowest-energy Γ_n state ($N = 1$–5) will be numbered 1 and the second lowest Γ_n state 2, etc. The crystal-field states of the same symmetry (but of different *J*) may be mixed by the crystal-field potential, and so the Γ_N labels remain as good quantum numbers.

TABLE 1
Electric Dipole Selection Rules in D_{2d} Symmetry

D_{2d}	Γ_1	Γ_2	Γ_3	Γ_4	Γ_5
Γ_1				π	σ
Γ_2			π		σ
Γ_3		π			σ
Γ_4	π				σ
Γ_5	σ	σ	σ	σ	π

Since J-mixing does occur and some levels contain more than one J component, the Am^{3+} states will be labeled by the largest J component. The selection rules for electric dipole transitions in D_{2d} symmetry are consigned in Table 1. Since the experiments have been carried out on powdered samples, no polarized spectra could be recorded. Nevertheless, the D_{2d} selection rules have been considered. The ground multiplet $^7F_0$ has a Γ_1 symmetry, and then only the transitions between the fundamental Γ_1 and the Γ_4 and Γ_5 crystal-field levels can be observed in the excitation spectra. Zeeman effect has been used to observe the splitting of the doubly degenerated levels Γ_5.

EXPERIMENTAL RESULTS AND ANALYSIS OF THE SPECTRA

Fluorescence Spectrum

Excitation in the most intense absorption line at 19,941 cm^{-1} in the $^5L_6$ sublevel was used to get the luminescence spectrum at low temperature. Figure 1 shows the emission spectrum of $Am^{3+}/LiYF_4$ in the visible at 30 and 10 K. In this figure, two main groups of intense narrow lines are observed. Those most intense between 13,900 and 14,500 cm^{-1} correspond to the transitions $^5D_1 \rightarrow {}^7F_1$ and $^5L_6 \rightarrow {}^7F_2$, while the group of lines between 11,500 and 12,200 cm^{-1} corresponds to the transition $^5D_1 \rightarrow {}^7F_2$. In both groups, doublets are observed at 300 K. When the temperature decreases (see Fig. 1), the highest energy line disappears. The doublets are attributed to transitions originating from the two crystal-field levels of $^5D_1$ (Γ_2 and Γ_5) toward $^7F_1$ and $^7F_2$ multiplets.

In the particular case of Am^{3+}, transitions coming from $^5D_1$ and $^5L_6$ to different ^7F_n multiplets can overlap in the visible region. For example, $^5D_1 \rightarrow {}^7F_1$ transitions overlap with $^5L_6 \rightarrow {}^7F_2$ transitions (17), particularly in fluoride compounds where the rather low phonon cutoff (550 cm^{-1}) decreases the nonradiative processes rate and increases the radiative processes rate for the $^5L_6$ excited levels. Measurement of radiative decay time on the emission lines allows us to confirm the origin of the emission lines. The $^5L_6$ level has a very short lifetime, while the $^5D_1$ level has a long lifetime (17). The decay time measured on the lines at 14,510 and 17,167 cm^{-1} (1.5 ms) is characteristic of the crystal-field levels of the $5D_1$ multiplets and short lifetimes measured at 7 μs are characteristic of transitions originating from the $^5L_6$ sublevels. Most of the transitions originates from the $^5D_1$ level except the lines observed at 16,598 and 16,474 cm^{-1} and the weak band around 14,080 cm^{-1}.

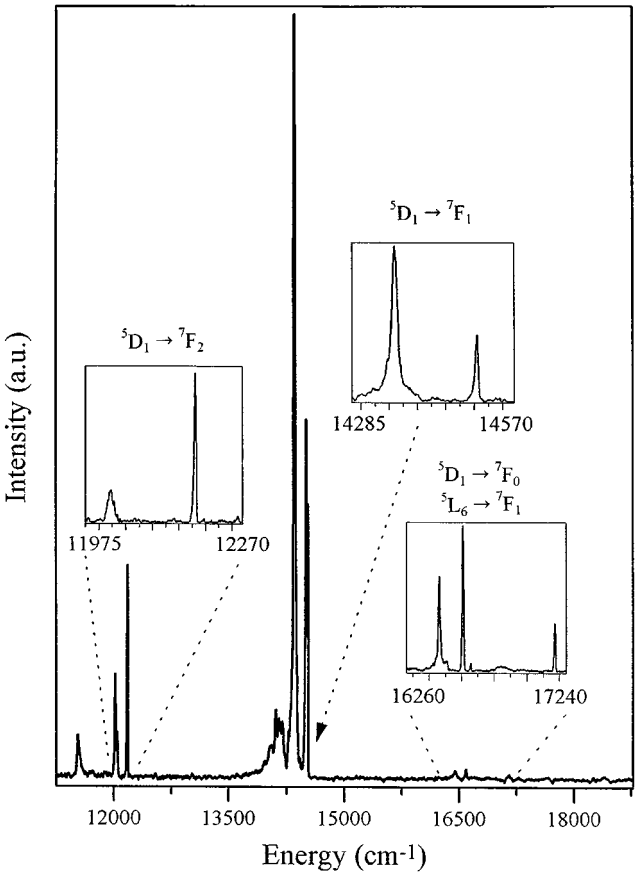

FIG. 1. Fluorescence spectrum of $Am^{3+}/LiYF_4$ in the visible at 30 K. (Insert figures are recorded at 10 K.)

Emission spectra were obtained under magnetic field at low temperature, to observe the splitting of the doubly degenerated levels Γ_5. To assign the maximum of excited states, the selection rules in D_{2d} was used. Since the multiplets with $J = 1$ are splitted by the crystal field in 2 sublevels $1\Gamma_2$ and $1\Gamma_5$, from the selection rules in D_{2d} we expect to see for the $^5D_1 \rightarrow {}^7F_1$ transitions three transitions $\Gamma_2 \rightarrow \Gamma_5, \Gamma_5 \rightarrow \Gamma_2$, and $\Gamma_5 \rightarrow \Gamma_5$. Under magnetic field, the twofold degenerated levels Γ_5 should be splitted or broadened. The line at 14,510 cm^{-1} is clearly splitted when the magnetic field is increased up to 5.47 T, indicating that this transition comes from a Γ_5 level. However, the line at 14,354 cm^{-1} does not change. Then the peaks at 14,532 and 14,510 cm^{-1} were attributed to the $\Gamma_2 \rightarrow \Gamma_5$ and $\Gamma_5 \rightarrow \Gamma_5$ transitions. Since the $\Gamma_2 \rightarrow \Gamma_2$ is forbidden by the selection

rules in D_{2d}, the last level at 14,354 cm^{-1} can only be attributed to the $\Gamma_5 \rightarrow \Gamma_2$ transition. The energy difference between maxima in the doublets gives the crystal-field splitting of the $^5D_1$ multiplet which is only 22 cm^{-1}.

In the region between 16,130 and 17,240 cm^{-1}, we observe several peaks attributed to the transitions $^5D_1 \rightarrow {}^7F_0$ and $^5L_0 \rightarrow {}^7F_1$. For the first transition, only $\Gamma_5 \rightarrow \Gamma_1$ is allowed. It corresponds to the peak at 17,167 cm^{-1}. Then we can deduce the energy of the crystal-field sublevels $^7F_1$ at 2666.1 cm^{-1} (Γ_5) and 2811 cm^{-1} (Γ_2), and $^5D_1$ at 17,167.1 cm^{-1} (Γ_5) and 17,188.7 cm^{-1} (Γ_2). The narrow lines observed at 16,601 and 16,456 cm^{-1} correspond to $^5L_6 \rightarrow {}^7F_1$ (Γ_2, Γ_5) transitions. Then, these transitions originate from the $^5L_6$ sublevel at 19,272 cm^{-1} for which the symmetry can be either Γ_5 or Γ_3. At the lowest energy part of the line at 14,364 cm^{-1}, the weaker band corresponds to an emission originating from the $^5L_6$ sublevel toward the $^7F_2$ multiplet.

In the infrared region, several groups of lines are observed (Fig. 2), while between 12,200 and 11,400 cm^{-1}, the three lines are attributed to $^5D_1 \rightarrow {}^7F_2$ ($\Gamma_1, \Gamma_3, \Gamma_4, \Gamma_5$) transitions, the group of weaker lines between 8300 and 9500 cm^{-1} corresponds to the $^5D_1 \rightarrow {}^7F_3$ transitions, the group of lines between 7200 and 7800 cm^{-1} correspond to the $^5D_1 \rightarrow {}^7F_4$ transitions, and the weaker lines observed between 5200 and 6600 cm^{-1} are attributed to the $^5D_1 \rightarrow {}^7F_5$ transitions. Except for the first group of lines, all these transitions are observed for the first time for Am^{3+}. Decay time measured on these emitting levels indicates that they originate from the $^5D_1$ sublevel. At 4 K, the three lines at 12,188, 12,028, and 11,561 cm^{-1} allow one to deduce three $^7F_2$ sublevels at 4975.7, 5134.8, and 5600 cm^{-1}. At higher temperature, a second peak arises at 22 cm^{-1}, at the highest energy side from the second line. The only irreducible representation for $^7F_3$ sublevel, for which both transitions coming from the Γ_5 and Γ_2 ($^5D_1$) multiplets are allowed in D_{2d} symmetry, can only be Γ_3. For the other emission lines observed in the infrared, the energy of the $^7F_3$ and $^7F_4$ sublevels was determined assuming that the transitions originate from the lowest energy sublevel of $^5D_1$ (Γ_5). They were deduced to be at 7443.5, 7511.4, and 7602 cm^{-1} for the $^7F_3$ multiplet and 9390.8, 9596.4, 9719.9, and 9791.5 cm^{-1} for the $^7F_4$ multiplets. However, no assignment could be deduced for this multiplet from the selection rules. The peaks observed between 6600 and 5400 cm^{-1} allow to deduce $^7F_5$ sublevels at 10,901.8, 10,929.3, 11,030.4, 11,396.3, 11,518.8, and 11,586.9 cm^{-1}.

Then from the numerous transitions observed in the infrared spectrum, and coming mostly from the lowest energy sublevel $^5D_1$ (Γ_5), 19 crystal field levels were deduced for the $^7F_2$, $^7F_3$, $^7F_4$, and $^7F_5$ multiplets. All together with the visible region, 21 sublevels were obtained.

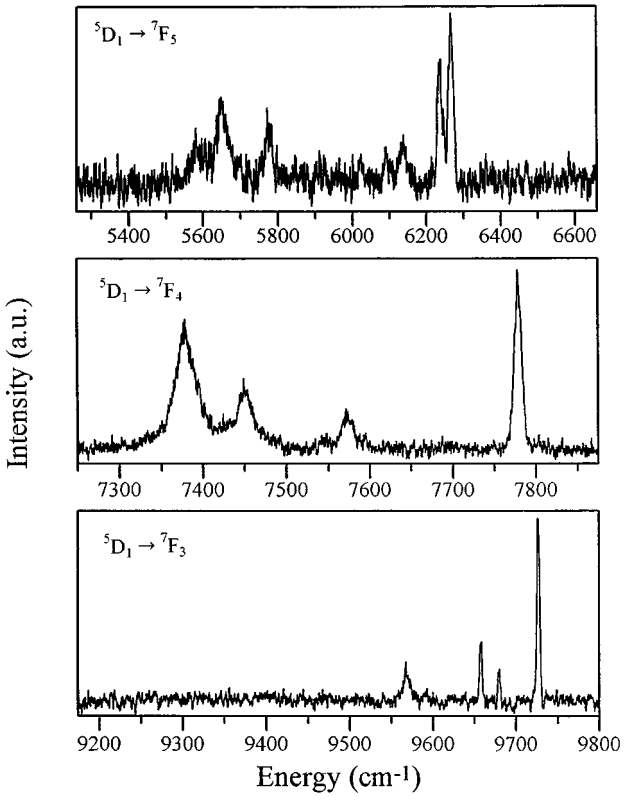

FIG. 2. Fluorescence spectrum of $Am^{3+}/LiYF_4$ in the infrared at 10 K.

Excitation Spectra

In Fig. 3, the low temperature excitation spectra obtained by monitoring the most intense fluorescence line at

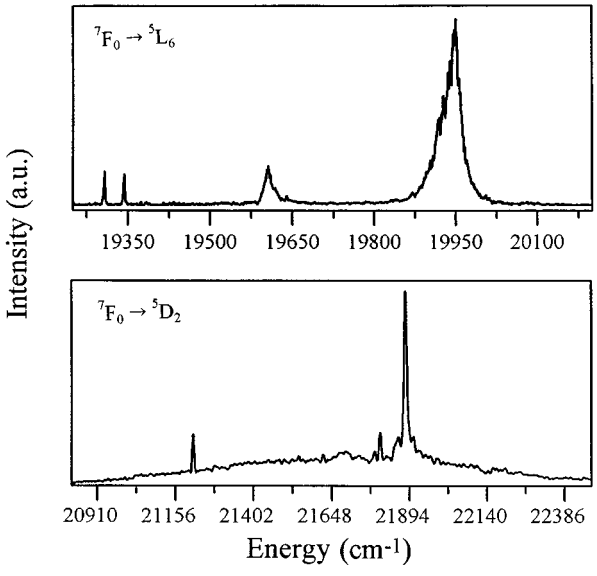

FIG. 3. Excitation spectra of $Am^{3+}/LiYF_4$ at 10 K.

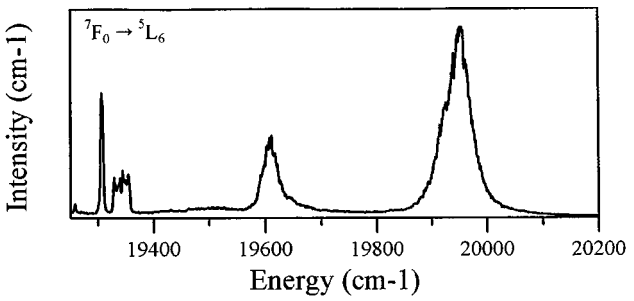

FIG. 4. Excitation spectrum of $^7F_0 \rightarrow {}^5L_6$ under magnetic field ($B = 5.4$ T) at 10 K.

14,363 cm^{-1} are presented. The regions 19,230–20,400 cm^{-1} and 20,800–22,200 cm^{-1} correspond to the transitions from the Γ_1 ($^7F_0$) ground level to respectively the $^5L_6$ and $^5D_2$ manifolds multiplets. In the excitation spectra, only the transitions $\Gamma_1 \rightarrow \Gamma_4$ and $\Gamma_1 \rightarrow \Gamma_5$ are allowed by the selection rules in D_{2d}. So in the region of the $^5L_6$ levels, five levels ($2\Gamma_4$, and $3\Gamma_5$) should be observed. Between 19,230, and 20,200 cm^{-1}, two narrow lines and two broad lines are observed at 19,296, 19,339, 19,588, and 19,938 cm^{-1}. Between 20,800 and 22,200 cm^{-1}, most of the narrow lines 21,881, 21,803, and 21,213 cm^{-1} correspond to the $^7F_0$ (Γ_1) $\rightarrow {}^5D_2$, $^5G_2$ ($\Gamma_{4,5}$) transitions. In order to identify the symmetry (Γ_4 or Γ_5) of the $^5L_6$ sublevels, Zeeman experiments have been carried out. Figure 4 shows the Zeeman excitation spectrum (with a magnetic field of 5.7 T) in the $^5L_6$ multiplet energy region. When the magnetic field is increased, a large splitting occurs on the narrow line at 19,335 cm^{-1}. However, there is no obvious change in the shape of the other lines.

DISCUSSION

From the fluorescence spectra and the excitation spectra, only one site was observed for Am^{3+}, and 29 levels could be assigned in the D_{2d} symmetry. All the levels were then fitted by full diagonalization of the free ion and crystal-field Hamiltonians given earlier.

The computations were performed in three steps. The first consisted of an approximate determination of the Slater parameters F^k and the spin–orbit constant ζ, the crystal-field parameters being fixed at zero. The initial free ion values where those calculated for Am^{3+} in ThO_2 (15). These calculations were carried out using the experimental excited levels deduced from the optical spectra and by picking out the barycenters and assigning the LSJ values. Then, the crystal-field parameters were determined using the experimental energies of the Stark components of the $^7F_1$, $^7F_2$, $^7F_3$, $^7F_4$, $^7F_5$, and $^5D_1$ multiplets. The starting, values were the same as those calculated for U^{3+} in $LiYF_4$ (15). The final step consisted of fitting all the energy levels, in both

TABLE 2
Calculated and Experimental Energy Levels

Level	Largest S–L–J comp.	Calc. energy (cm^{-1})	Exp. energy (cm^{-1})	($E_{exp}E_{cal}$) (cm^{-1})
Γ_1	$^7F_0$	2.8	0.0	− 2.8
Γ_5	$^7F_1$	2695.5	2666.1	− 29.4
Γ_2	$^7F_1$	2811.6	2811.0	− 0.6
Γ_4	$^7F_2$	4975.3	4975.7	0.4
Γ_5	$^7F_2$	5142.9	5134.8	− 8.1
Γ_1	$^7F_2$	5584.4	5595.0	10.6
Γ_3	$^7F_2$	5623.5		
Γ_4	$^7F_3$	7452.5		
Γ_2	$^7F_3$	7480.3	7443.5	− 36.8
Γ_5	$^7F_3$	7491.6	7511.4	19.8
Γ_5	$^7F_3$	7591.5	7602.0	− 10.5
Γ_3	$^7F_3$	7842.7		
Γ_1	$^7F_4$	8818.2		
Γ_5	$^7F_4$	9371.5	9390.8	19.3
Γ_2	$^7F_4$	9509.5		
Γ_3	$^7F_4$	9637.5	9596.4	− 41.1
Γ_4	$^7F_4$	9708.0	9719.9	11.9
Γ_5	$^7F_4$	9788.5	9791.5	3.0
Γ_1	$^7F_4$	9984.5		
Γ_4	$^7F_5$	10867.8	10901.8	33.0
Γ_5	$^7F_5$	10919.0	10929.3	10.3
Γ_2	$^7F_5$	11064.7	11030.4	− 34.3
Γ_5	$^7F_5$	11349.4		
Γ_1	$^7F_5$	11395.0		
Γ_2	$^7F_5$	11396.0	11396.3	− 0.3
Γ_5	$^7F_5$	11518.0	11518.0	− 0.8
Γ_3	$^7F_5$	11569.2	11586.9	17.7
Γ_1	$^7F_6$	12258.8		
Γ_5	$^7F_6$	12345.5		
Γ_4	$^7F_6$	12345.8		
Γ_1	$^5D_0$	12349.9		
Γ_2	$^7F_6$	12609.6		
Γ_5	$^7F_6$	12630.0		
Γ_3	$^7F_6$	12694.8		
Γ_4	$^7F_6$	12696.8		
Γ_1	$^7F_6$	12701.2		
Γ_5	$^7F_6$	12729.3		
Γ_3	$^7F_6$	12733.5		
Γ_5	$^5D_1$	17147.8	17167.1	19.7
Γ_2	$^5D_1$	17226.2	17188.7	− 37.5
Γ_3	$^5L_6$	19284.8	19274.0	− 10.8
Γ_4	$^5L_6$	19328.4	19298.6	− 30.2
Γ_5	$^5L_6$	19393.7	19334.4	− 59.3
Γ_2	$^5L_6$	19424.1		
Γ_3	$^5L_6$	19438.2		
Γ_5	$^5L_6$	19553.3	19597.6	44.3
Γ_2	$^5L_6$	19634.9		
Γ_1	$^5L_6$	19768.4		
Γ_5	$^5L_6$	19793.0		
Γ_4	$^5L_6$	19870.2	19941.1	70.1
Γ_4	$^5D_2$	21136.8	21207.0	70.8
Γ_1	$^5D_2$	21329.8		
Γ_4	$^5G_2$	21575.9		
Γ_5	$^5D_2$	21693.8		
Γ_5	$^5G_2$	21742.6		
Γ_4	$^5D_2$	21769.2		
Γ_4	$^5G_2$	21837.9	21797.0	− 40.9
Γ_4	$^5H2_3$	21900.1	21875.0	− 25.1
Γ_5	$^5H2_3$	22114.8		
Γ_3	$^5G_2$	22137.1		
Γ_3	$^5H2_3$	22340.7		

TABLE 3
Energy Parameters for $LiYF_4$: Am^{3+}

Parameters	cm^{-1}
F^2	49798 (155)
F^4	41134 (179)
F^6	30350 (156)
ξ	2567 (18)
α	32 (8)
β	[− 660]
γ	[1000]
B_0^2	473 (47)
B_0^4	− 1736 (55)
B_4^4	− 2253 (61)
B_0^6	80 (9)
B_4^6	− 2222 (75)
T^2	[200]
T^3	[50]
T^4	[40]
T^6	[− 360]
T^7	[390]
T^8	[340]
M^0	[0.99]
M^2	[0.55]
M^4	[0.38]
P^2	[850]
P^4	[637]
P^6	[425]
rms	38

Note. All parameters values in [ ] were held fixed in the fitting procedure.

infrared and visible regions, varying the free ion and the crystal-field parameters simultaneously (except the $\alpha, \beta, \gamma, P^k, M^k, T^k$ parameters which were held fixed at the values used for Am^{3+} in ThO_2). The results of the fit and the final assignment of the experimental levels are given in Table 2. The spectroscopic parameters are given in Table 3.

The set of the crystal-field parameters is quite satisfactory. It gives good agreement between calculated levels and experimental levels, with an rms of 38 cm^{-1} for 29 levels. Compared to the spectroscopic parameters obtained for U^{3+} in the same matrix, the crystal field parameters have the same order of magnitude, except the B_4^6 parameter which is larger (absolute value) for U^{3+} ($5f^3$) than for Am^{3+} ($5f^6$). The ratios such as B_0^4/B_4^4 or B_0^6/B_4^6, which correspond to the ratio $A_q^k/A_{q'}^k$ should depend only on the host structure site, if the distortion due to the doping can be neglected. Thus, the comparison between the values found for Am^{3+}, U^{3+}, Eu^{3+}, and Nd^{3+} in $LiYF_4$ could be a way to check the validity of the fitting (21). Table 4 indicates that all the ratios are roughly the same. In the case of Eu^{3+}, two different values are obtained for the ratio B_0^6/B_4^6, corresponding to different parameters calculated in the literature (2, 4). The fitted values of B_0^6 are close to zero and then smaller than the error in the parameter, so the ratio obtained for this ion cannot be meaningful.

TABLE 4

	Am^{3+}	Eu^{3+}	U^{3+}	Nd^{3+}
B_0^4/B_4^4	0.76	0.78	0.86	0·82
B_0^6/B_4^6	− 0.037	− 0.006[2] − 0.044[4]	− 0.028	− 0.027

To compare the magnitude of the crystal-field effect for the Eu^{3+} ion and the Am^{3+} ion, N_v parameter of Auzel and Malta (24) described below can be used.

$$N_v = \left[\sum (B_q^k)^2 \frac{4\pi}{2k+1} \right]^{1/2}$$

This parameter allows a comparison to be made of the strength of crystal-field interaction on different f^n ions in the same host and a particular f^n ion in different host. In (19), the authors show that the ratio of N_v between an actinide and the isoelectronic lanthanide ion in the same host matrix is on the order of 2.2–2.4, whatever the matrix. Some values of N_v and the ratio $N_v(5f^n)/N_v(4f^n)$ in different hosts such as ThO_2, $LaCl_3$, and $LiYF_4$ are given Table 5. These results indicate that the value for Am^{3+} in $LiYF_4$ is consistent with the previous studies.

CONCLUSION

Although the sample was polycrystalline powder, polarization could not be used for assigning the symmetry of the excited levels, however, using the selection rules in D_{2d} and Zeeman experiments, most of the crystal-field levels deduced from the emission and excitation spectra could be labelled. The phenomenological parameters have been calculated assuming that S_4 could be approximated in the

TABLE 5
N_v Parameters

Ion	$Am^{3+}(Eu^{3+})$	$Am^{3+}(Eu^{3+})$	$Am^{3+}(Eu^{3+})$	$U^{3+}(Nd^{3+})$
Host	ThO_2	$LaCl_3$	$LiYF_4$	$LiYF_4$
Symmetry	O_h	D_{3h}	S_4	S_4
Reference	(18) (18)	(20) (25)	This work (4)	(15) (1)
N_v (cm^{-1})	10439 (4296)	2297 (1042)	5355 (2147)	7230 (2876)
$\frac{N_v\ (5f^n)}{N_v\ (4f^n)}$	2.43	2.20	2.49	2.5

D_{2d} symmetry. A least-square adjustment yields a mean error of 38 cm^{-1} with 29 levels. The crystal-field strength for Am^{3+} is 2.5 times larger than for Eu^{3+} in the same matrix.

ACKNOWLEDGMENTS

The authors are grateful to Pr. M. Reid for the use of his computer program for the fitting procedure.

REFERENCES

1. A. A. S. Da Gama, G. FD. De Sa, P. Porcher, and P. Caro, *J. Chem. Phys.* **75,** 2583 (1981).
2. C. K. Jayasankai, M. F. Reid, and F. S. Ridchardson, *Phys. Stat. Sol. B* **155,** 559 (1989).
3. M. Malinowski, B. Jacquier, M. Bouazaoui, M. F. Joubert, and C. Linares, *Phys. Rev. B* **41,** 31 (1990).
4. C. Görller-Wallrand, M. Behers, P. Porcher, and W. T. Carnall, *J. Less Com. Met.* **120,** 271 (1986).
5. C. Görller-Wallrand, and L. Fluyt, *J. Less Com. Met.* **148,** 339 (1989).
6. S. A. Payne, L. L. Chase, L. A. Smith, W. L. Kway, and W. F. Krupke, *IEEE J. Quant. Elect.* **28,** 2619 (1992).
7. H. Hemmet, *Opt. Lett.* **14,** 435 (1989).
8. S. Hubert, D. Meichenin, B. W. Zhou, and F. Auzel, *J. Lum.* **50,** 7 (1991).
9. F. Auzel, S. Hubert, and D. Meichenin, *Appl. Phys. Lett.* **54,** 681 (1989).
10. A. M. Tkatchuk, A. V. Poletimova, and M. V. Pekov, *Opt. Spectrosc.* **59,** 680 (1985).
11. G. J. Quarles, L. Esterowitz, G. M. Rosenblat, R. Uhrin, and R. F. Belt, *OSA Proc. Adv Solid State Lasers* **13,** 306 (1992).
12. E. Simoni, M. Louis, S. Hubert, and M. F. Reid, *J. Phys. II* **5,** 755 (1995).
13. S. Hubert, M. Louis, E. Simoni, W. P. Zhang, and J. Y. Gesland, *J. Lum.* **60&61,** 245 (1994).
14. D. Meichenin, F. Auzel, S. Hubert, E. Simoni, M. Louis, and J. Y. Gesland, *Electron. Lett.* **30,** 1309 (1994).
15. E. Simoni, M. Louis, J. Y. Gesland, and S. Hubert, *J. Lum.* **65,** 153 (1995).
16. W. T. Carnall and H. M. Crosswhite "Optical spectra and electronic structure of actinide ions in compounds and in solution." Report ANL-84-90.
17. R. W. Valenzuela and R. T. Brundage, *J. Chem. Phys.* **93,** 8469 (1990).
18. R. T. Brundage, M. M. Svatos, and R. Grinbergs, *J. Chem. Phys.* **95,** 7933 (1991).
19. S. Hubert, Thouvenot, and N. Edelstein, *Phys. Rev. B* **48,** 5751 (1993).
20. P. Thouvenot, S. Hubert, and N. Edelstein, *Phys. Rev. B* **50,** 9715 (1994).
21. W. T. Carnall, *J. Less-Common Met.* **156,** 221 (1989).
22. G. P. Chudnovskya, Yu. I. Gavrish, and Yu. A. Barbanel, *Radiokhimiya* **30,** 46 (1988).
23. G. P. Chudnovskya, R. B. Duskin, V. V. Kolin, and Yu. A. Barbanel, *Radiokhimiya* **27,** 545 (1985).
24. F. Auzel and O. L. Malta, *J. Phys.* **44,** 201 (1983).
25. W. T. Carnall, "Systematic analysis of the spectra of trivalent actinide chloride in D_{3h} site symmetry." Report ANL-89/39.